Taylor & Francis
Taylor & Francis Group

Mechanics of Advanced Materials and Structures

ISSN: (Print) (Online) Journal homepage: www.tandfonline.com/journals/umcm20

Piezoelectric transducer-assisted mass normalization of mode shapes in thin-walled structures

Seyed Morteza Hoseyni, Amirreza Aghakhani & Ipek Basdogan

To cite this article: Seyed Morteza Hoseyni, Amirreza Aghakhani & Ipek Basdogan (03 Feb 2025): Piezoelectric transducer-assisted mass normalization of mode shapes in thin-walled structures, Mechanics of Advanced Materials and Structures, DOI: 10.1080/15376494.2025.2460088

To link to this article: https://doi.org/10.1080/15376494.2025.2460088

© 2025 The Author(s). Published with license by Taylor & Francis Group, LLC

Published online: 03 Feb 2025.

Submit your article to this journal

View related articles

View Crossmark data

Full Terms & Conditions of access and use can be found at
https://www.tandfonline.com/action/journalInformation?journalCode=umcm20

MECHANICS OF ADVANCED MATERIALS AND STRUCTURES
https://doi.org/10.1080/15376494.2025.2460088

Taylor & Francis
Taylor & Francis Group

ORIGINAL ARTICLE

OPEN ACCESS Check for updates

Piezoelectric transducer-assisted mass normalization of mode shapes in thin-walled structures

Seyed Morteza Hoseyni[a,b], Amirreza Aghakhani[c], and Ipek Basdogan[a]

[a]Mechanical Engineering Department, College of Engineering, Koc University, Istanbul, Turkey; [b]Acoustics Research Centre, University of Salford, Salford, UK; [c]Institute of Biomaterials and Biomolecular Systems, University of Stuttgart, Stuttgart, Germany

ABSTRACT

This paper introduces a robust and accurate, yet simple and straightforward technique for measuring mass-normalization scale factor for each vibration mode of thin-walled structures using a piezoelectric transducer. The methodology relies on electromechanical impedance measurement and the charge frequency response function of a piezoelectric transducer attached to the structure which leads to the determination of the mass-normalized component of mode shape at the force location i.e. reference point. The scaling factor for each vibration mode is determined by comparing the arbitrary mode shape with the mass-normalized one at the reference point.

ARTICLE HISTORY
Received 9 October 2024
Accepted 25 January 2025

KEYWORDS
Experimental modal analysis; mass normalized mode shape; scaling factor; piezoelectric; admittance measurement

1. Introduction

Using vibrations to detect structural damage has become common in the field of structural health monitoring in recent years. This has led to significant research into practical modal analysis, as it offers an effective and cost-efficient approach [1, 2]. It involves the identification of any variations on structure's modal parameters because any structural defect can alter the vibrational behavior of the system. One particularly promising approach is mode shape identification, which not only serves to detect the presence of damage but also facilitates discovering the specific location of the defect by establishing a Damage Location Indicator using the curvatures of the normalized mode shape [3–5]. Damage characterization using modal identification can be enhanced by artificial intelligence to determine not only the location but also the size of the damage on delaminated composite structures [6]. However, it is crucial to obtain the mass-normalized mode shape of the structure to ensure the accuracy and reliability of the analysis [7–9].

Avitabile [10] presented a thorough and detailed overview of various techniques employed in modal identification methods. Modal properties of a structure depend on the material and the geometry of the structure [11]. Modal identification refers to determining natural frequencies, modal damping, and mode shapes of the structure. This can be conducted with two different practical approaches. The availability of both input and output data leads to experimental modal analysis (EMA) [12]. On the other hand, identification of modal parameters based on only the response of the structure refers to operational modal analysis (OMA). This approach is mostly used in large-scale structures where the source of the excitation is ambient vibration and difficult to be measured [12]. The response-based frequency response function has been utilized to identify additional poles of a structural system, aiding in structural analysis and localized diagnostics [13]. Modal analysis of rotating viscoelastic sandwich beams was investigated to explore the effects of rotation speed, thickness, core layer position, and shear modulus frequency dependence on dynamic characteristics under various boundary conditions [14]. An experimental modal analysis method has been presented for a plate structure using a roving inertial shaker. The superiority of this method to the roving hammer method was proved by determining higher number of modes with higher stability [15]. Experimental modal analysis of a single-link flexible manipulator have been investigated based on several time-domain system identification approaches [16]. A novel approach for experimental vibroacoustic modal analysis has been developed to determine the modal parameters of a plate-cavity system. The frequency response function was acquired from the roving hammer test and nonlinear curve fitting was used to identify the modal parameters of the structure [17]. A machine learning-assisted automated operational modal analysis approach was introduced based on the output response of linear structures and validated for a tower [18]. Despite the claim that the EMA is more reliable approach for modal identification

CONTACT Seyed Morteza Hoseyni s.hoseyni@salford.ac.uk Mechanical Engineering Department, College of Engineering, Koc University, Istanbul 34450, Turkey.

© 2025 The Author(s). Published with license by Taylor & Francis Group, LLC
This is an Open Access article distributed under the terms of the Creative Commons Attribution-NonCommercial-NoDerivatives License (http://creativecommons.org/licenses/by-nc-nd/4.0/), which permits non-commercial re-use, distribution, and reproduction in any medium, provided the original work is properly cited, and is not altered, transformed, or built upon in any way. The terms on which this article has been published allow the posting of the Accepted Manuscript in a repository by the author(s) or with their consent.

[19, 20], it is proved that both approaches provide sufficient accuracy on obtaining modal parameters [21].

Mode shapes obtained with modal identification methods are arbitrarily scaled. However, there are unique eigenvectors known as mass normalized mode shapes which represent unique properties of the structure and offer a valuable representation of the structure behavior [7]. Therefore, researchers are motivated to develop novel techniques for the mass normalization of the mode shapes. A sensitivity-based method for mass-normalizing operational mode shapes was presented [22]. This method involves adding known masses to a test structure and measuring the natural frequency shifts. It was applied to a beam-like structure [22] and a civil structure, namely a bridge [23]. Mass-change strategy was also implemented to experimental modal analysis aiming to mass normalize the displacement and strain mode shapes of a free-free beam [24]. A scaling factor determination method was developed based on changing both mass and stiffness of the structure which improves the mass normalizing of the first mode shape [25]. However, the value of additional mass and spring should be specified carefully to avoid significant changes in the mode shapes. Additionally, these methods are dependent on the nodal points of the vibration mode and requires performing several experiments where in each test the mass or spring is located at different points of the structure [22]. A finite element-based approach was introduced to predict the scaling factor of mode shapes obtained by operational modal analysis [26]. Although this approach predicts the mass normalized mode shapes better when compared with the mass-change approaches, it requires precise knowledge of the material properties of the structure [26]. In another study, a mass normalization method was introduced which used just one sensor on a vehicle aiming to identify the mode shapes with high spatial resolution and to reduce the sensitivity to the road roughness [27]. A pair of single sensor and actuator—either not collocated or collocated—was used to mass normalize the mode shape of a bridge structure based on input-output balance [28]. Input and output data was measured in time domain and pseudo-modal response was developed to estimate the mass normalized mode shapes.

The mass normalization methods are mostly developed for large-scale structures i.e. bridges and towers. In the case of thin-walled structures, a novel method is required to predict a scale factor without changing the mode shapes by adding extra mass to the structure. On the other hand, the conventional methodology for determining mass normalized mode shapes of structures by experimental modal analysis requires precise calculation of modal parameters which requires calculation costs. Therefore, in this paper, a new method is presented for thin-walled structures which avoids additional mass usage and reduces excessive calculations through complex equations. Unlike the methods introduced in the literature, this methodology consists of a few tests and does not require any information about the material properties of the structure. It is based on electromechanical impedance measurement and the charge response of a piezoelectric transducer attached to the structure. The piezoelectric transducers are thin films which do not have a significant effect on the dynamic of the thin-walled structures. The application of piezoelectric transducers have been studied for vibration control [29], structural health monitoring [30], energy harvesting [31–34], human physiological signals monitoring [35], and mode shape identification of straight and curved beams [36]. The extraction of eigenvectors using a piezoelectric transducer is limited to an arbitrary scale of mode shapes. However, this study introduces a new application of piezoelectric transducer which can be implemented on modal identification methods to mass normalize the mode shapes of thin-walled structures i.e. beams and plates. It is applicable to the EMA where the input data can be measured. First, the structure is excited mechanically and the mechanical frequency response of the reference point i.e. force location, as well as the charge frequency response of piezoelectric is measured. In the second step, the electromechanical admittance of the piezoelectric attached to the structure is measured where there is no external mechanical excitation. The measured admittance provides information to obtain natural frequency, modal damping, and coupling factors of the system. Based on the identified parameters, the mass-normalized mode shape of the reference point can be easily obtained. The last step is to obtain the scaling factor considering the arbitrary mode shape and the mass normalized one at the reference point. Having the scaling factor of each vibration mode, the mass normalized mode shape of the entire structure at each mode can be obtained. The methodology is developed for a plate structure which can be used for beams as well.

2. Analytical background

The mechanical equation of motion for a piezoelectric integrated with a plate structure in modal coordinate is as follows [37]:

$$\frac{d^2\eta_m(t)}{dt^2} + 2\zeta_m\omega_m\frac{d\eta_m(t)}{dt} + \omega_m^2\eta_m(t) - \Theta_m v_p(t) = f(t)\varphi_m(x_0, y_0). \tag{1}$$

where $v_p(t)$ is the piezoelectric voltage, $\varphi_m(x_0, y_0)$ is the mass normalized mode shape at reference point, and (x_0, y_0) is the location of point force. ω_m, ζ_m, and Θ_m are, respectively, the natural frequency, the modal damping ratio, and the modal electromechanical coupling of the piezoelectric patch for the mth vibration mode. $\eta_m(t)$ is the time dependent modal coordinate of the plate. By dividing Eq. (1) by Θ_m and subsequently multiplying the first, second, and third terms by $\frac{\Theta_m}{\Theta_m}$, it can be reorganized as:

$$\frac{1}{{\Theta_m}^2}\frac{d^2}{dt^2}\left(-\Theta_m\eta_m(t)\right) + \frac{2\zeta_m\omega_m}{{\Theta_m}^2}\frac{d}{dt}\left(-\Theta_m\eta_m(t)\right) + \frac{\omega_m^2}{{\Theta_m}^2}\left(-\Theta_m\eta_m(t)\right) + v_p(t) = -\frac{f(t)\varphi_m(x_0, y_0)}{\Theta_m} \tag{2}$$

The term $-\Theta_m\eta_m(t)$ represents the charge response of the piezoelectric $q_m(t)$ [38] which describes how charge accumulates in response to mechanical excitation. Equation (2)

can be considered as equation of a second order circuit where the terms $\frac{1}{\Theta_m{}^2}$, $\frac{2\zeta_m\omega_m}{\Theta_m{}^2}$, and $\frac{\Theta_m{}^2}{\omega_m^2}$ are equivalent to inductance (L_m), resistance (R_m), and capacitance (C_m), respectively. Having substituted the equivalent electrical components and the charge response of piezoelectric into Eq. (2), the equivalent circuit equation of the piezoelectric can be obtained as:

$$L_m \frac{d^2}{dt^2}\left(q_m(t)\right) + R_m \frac{d}{dt}\left(q_m(t)\right) + \frac{1}{C_m}\left(q_m(t)\right) + v_p(t) = -\frac{f(t)\varphi_m(x_0, y_0)}{\sqrt{L_m}} \tag{3}$$

Short circuiting the piezoelectric electrodes, the piezoelectric voltage will be zero i.e. $v_p(t) = 0$. Considering that $\frac{1}{L_m C_m} = \omega_m{}^2$, Fourier transform of Eq. (3) can be calculated as:

$$R_m \cdot (j\omega_m) \cdot \tilde{Q}_{(j\omega_m)} = -\frac{\tilde{F}_{(j\omega_m)}\varphi_m(x_0, y_0)}{\sqrt{L_m}} \tag{4}$$

Where $\tilde{Q} = \mathcal{F}\{q_m\}$, and $\tilde{F} = \mathcal{F}\{f\}$ are the Fourier transforms of the piezoelectric output charge and force input, respectively. The ratio of output charge and input force in frequency domain represents the charge frequency response function (FRF) which is known as transfer function i.e. $\tilde{H}_{(j\omega_n)} = \frac{\tilde{Q}_{(j\omega_m)}}{\tilde{F}_{(j\omega_m)}}$. The mass normalized mode shape of the reference point can be obtained by rearranging Eq. (4) as:

$$\varphi_m(x_0, y_0) = \frac{R_m \cdot (j\omega_m)}{\sqrt{L_m}} \tilde{H}_{(j\omega_m)} \tag{5}$$

Identification of the equivalent electrical components can be conducted by measuring the admittance of the piezoelectric using an Impedance Analyzer device [39]. On the other hand, the charge transfer function of the piezoelectric can be obtained by exciting the structure with a shaker and measuring the voltage output of the piezoelectric at open circuit condition i.e. the electrodes of the piezoelectric are connected by a resistive load higher than 1 MΩ [39]. Using any modal identification method, the arbitrary mode shape of structure, including arbitrary mode shape component of the reference point $\Phi_m(x_0, y_0)$, can be obtained and the scaling factor can be calculated as:

$$S.F = \frac{\varphi_m(x_0, y_0)}{\Phi_m(x_0, y_0)} \tag{6}$$

Then the mass normalized mode shape of other degrees of freedom of the structure can be obtained as:

$$\varphi_m(x, y) = S.F \times \Phi_m(x, y) \tag{7}$$

3. Experiments

The proposed method for mass normalizing the mode shape was validated through experiments involving a fully clamped aluminum plate (CCCC) as the host structure, to which three piezo-patch harvesters (T105-A4E-602, produced by Piezo Systems, Inc.) were attached (see Figure 1). The piezoelectric transducer at the center of the plate is short circuited during all the experiments and has only mechanical contribution on the system. Material properties and dimensions of the plate and piezoelectric transducers are available at Table 1. Considering the nodal lines and mode shapes of each vibration mode, we conduct mass normalization for the first and second modes using PZT-1 (PZT-2 is short circuited), while PZT-2 is applied for mass normalization of the third mode (PZT-1 is short circuited). First, an experimental modal analysis was carried out to identify an arbitrary mode shape of the plate for the first three vibration modes, including the reference point as one of the measured degrees of freedom. The open circuit voltage FRF of the piezoelectric was measured and the charge FRF is calculated. The next step is to remove the shaker and measure the admittance of the piezoelectric to identify the equivalent electrical components of each vibration mode. The following sections provide detailed explanation of the procedure.

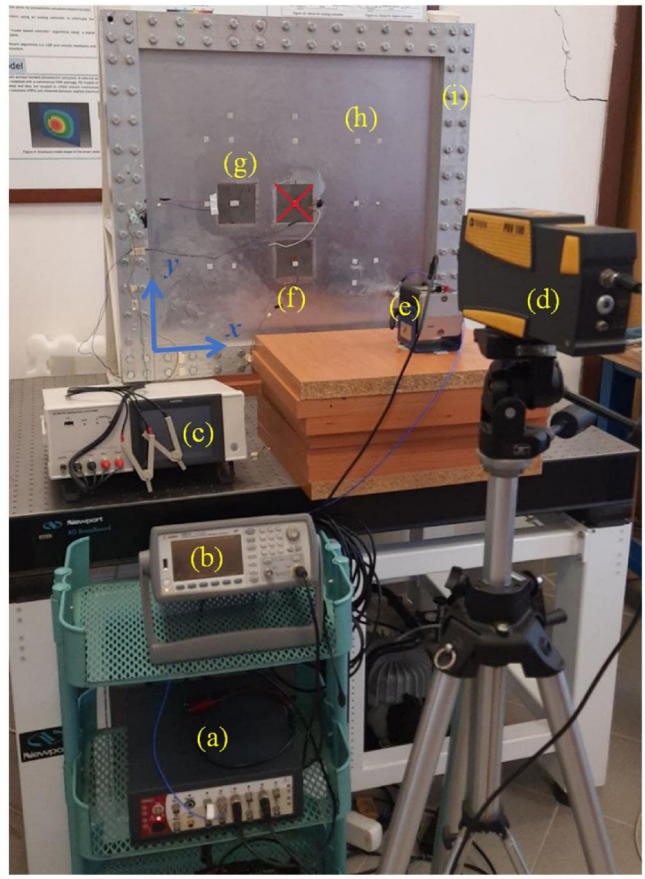

Figure 1. Experimental setup: (a) DAQ unit; (b) signal generator; (c) impedance analyzer; (d) PDV100 vibrometer; (e) shaker and a force transducer; (f) PZT-2; (g) PZT-1; (h) aluminum plate; and (i) clamping frame.

Table 1. Material properties and dimensions of experimental setup.

Property	Aluminum	Piezoceramic
Length (mm) X	580	72.4
Width (mm) Y	540	72.4
Thickness (mm)	1.9	0.267
Young's modulus (GPa)	65.1	66
Mass density (Kg/m^{-3})	2575	7800
Piezoelectric constant (pm/V)	–	−190
Permittivity constant (nF/m)	–	10.38

3.1. Experimental modal analysis

The experimental modal analysis of the plate was carried out considering 21 measurement points i.e. degree of freedom. The selection of test points was based on prior knowledge of the first, second, and third mode shapes of the plate. The structure was excited by a shaker with a force transducer (PCB 208C02) on the tip which measures the input force to the structure. The location of the input force i.e. reference point, is selected as $(x_0, y_0) = (495, 85)$ mm which is away from the nodal lines of three first mode shapes and can excite corresponding vibration modes. The test points and the reference points are demonstrated on Figure 2.

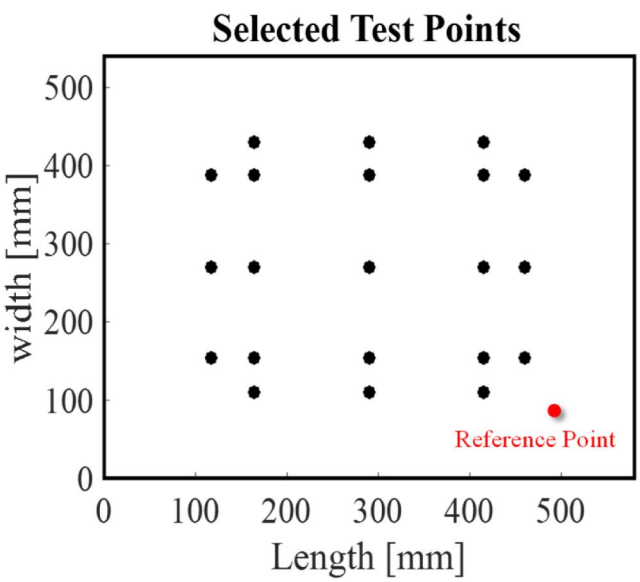

Figure 2. The location of test points and the reference point for experimental modal analysis.

The velocity FRF of the plate was measured by a PDV100 vibrometer while a swept sine signal was generated to excite the shaker at frequency range that includes the first three resonance frequencies of the plate. The swept signal is set to a level which avoids any nonlinearity in the dynamic of the structure. The acceleration FRFs can be easily obtained from the velocity FRFs. The mode shape identification method used in this study is based on the amplitude of the imaginary part of the acceleration FRF at resonance frequency [10]. The acceleration FRFs and their imaginary parts for all the test points are shown in Figure 3. It is worth noting that errors caused by noise and measurement inaccuracies can be minimized through careful calibration and averaging over repeated trials. However, the quality of measured FRFs should be ensured by checking the coherence and sufficiently high signal-to-noise ratio.

In an identical manner, experiments are performed to acquire the acceleration FRF of the reference point. Figure 4 shows the imaginary part of the acceleration FRF which identifies the arbitrarily scaled mode shapes components of the reference point for the first three vibration modes. During this experiment, the open-circuit output voltage FRF of the piezoelectric is measured as well. Having the internal capacitance of piezoelectric (C_0), the output charge response can be calculated from the open-circuit output voltage FRF [39]. It is worth noting that the mass normalizing process of first and second mode shapes has been carried out using PZT-1 where PZT-2 was used to mass normalize the third mode shape. Therefore, the voltage FRF of PZT-1 is

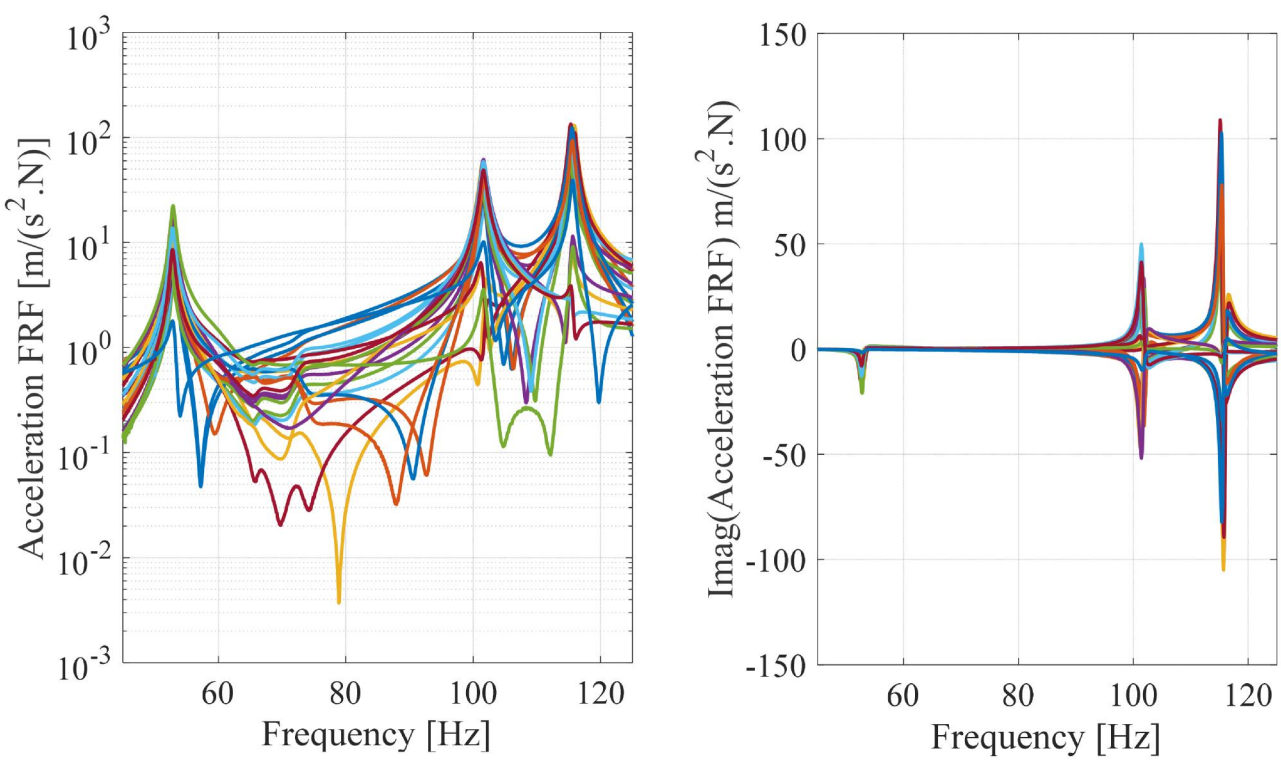

Figure 3. Acceleration FRF and its imaginary part for test points.

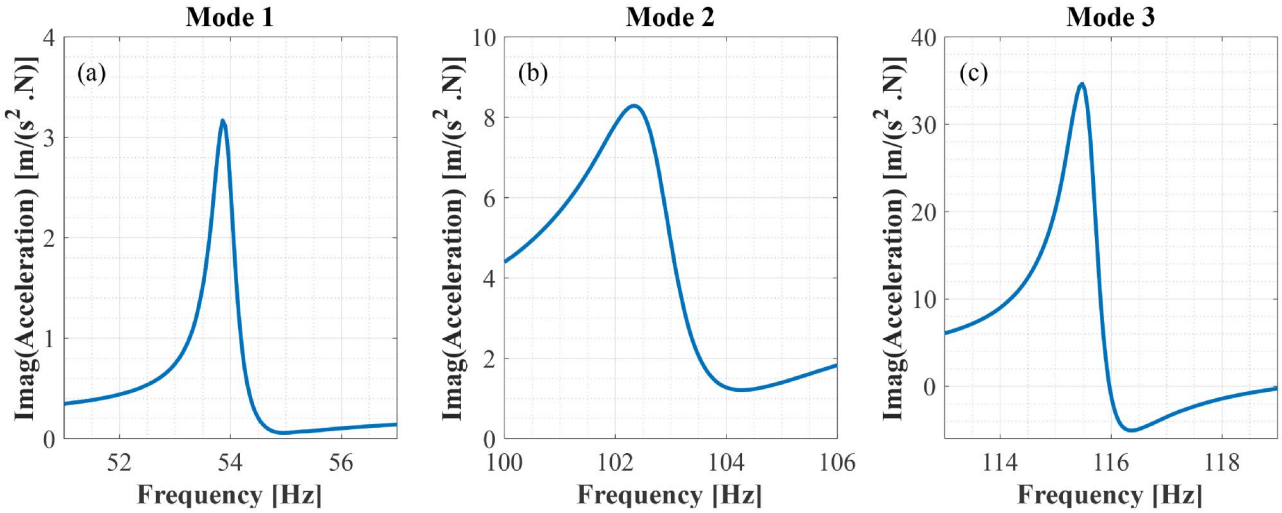

Figure 4. Imaginary part of acceleration FRF of reference point for (a) first mode, (b) second mode, and (c) third mode.

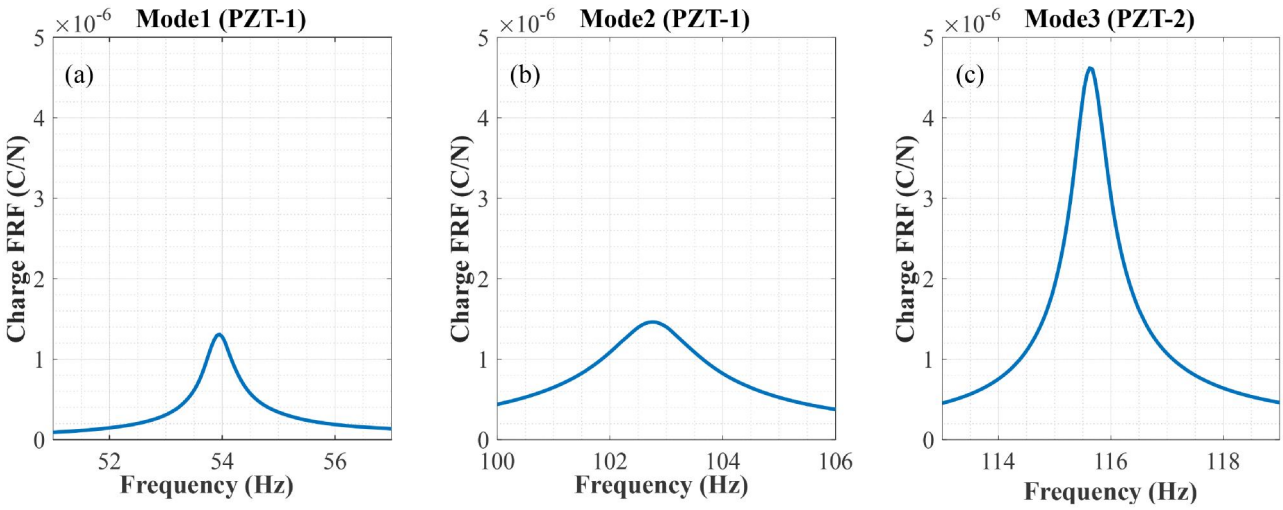

Figure 5. Output charge FRF of (a) PZT-1 around the first resonance, (b) PZT-1 around the second resonance, and (c) PZT-2 around the third resonance.

measured around the first and second resonance frequencies whereas the voltage FRF of PZT-2 was measured around the third resonance frequency. The output charge FRF of the PZT-1 around the first and second resonance, and the output of PZT-2 around the third resonance is shown in Figure 5.

3.2. Identification of the equivalent circuit components

The equivalent electrical components of the piezoelectric were identified based on measured admittance (Y) of transducer at each natural frequency. The value of measured admittance at each natural frequency can identify the equivalent resistor and internal capacitance of the piezoelectric where the real and imaginary parts correspond to the admittance of the equivalent resistor and the internal capacitance of the transducer, respectively. The value of the equivalent inductor can be determined by dividing the equivalent resistance by the difference between the frequencies at which resonance and antiresonance of the admittance occur. A detailed explanation of equivalent circuit identification from the measured admittance of piezoelectric is available at [39].

The admittance measurement of the piezoelectric transducer was carried out using HIOKI IM3570 which is also capable of calculating the equivalent electrical properties of the piezoelectric transducers. Figure 6 demonstrates the measured admittance and the equivalent electrical properties of PZT-1 around the first and second vibration modes, and PZT-2 around the third vibration mode.

4. Results and discussion

The mass-normalized mode shape of the reference point for three first vibration modes were determined through Eq. (5), which required measurements of the parameters of equivalent electrical components, charge FRFs, and resonance frequencies. Having the mass normalized mode shape and the arbitrary mode shape of the reference point, the scaling factor was identified for each vibration mode following Eq. (6). The measured parameters of the system and the determined

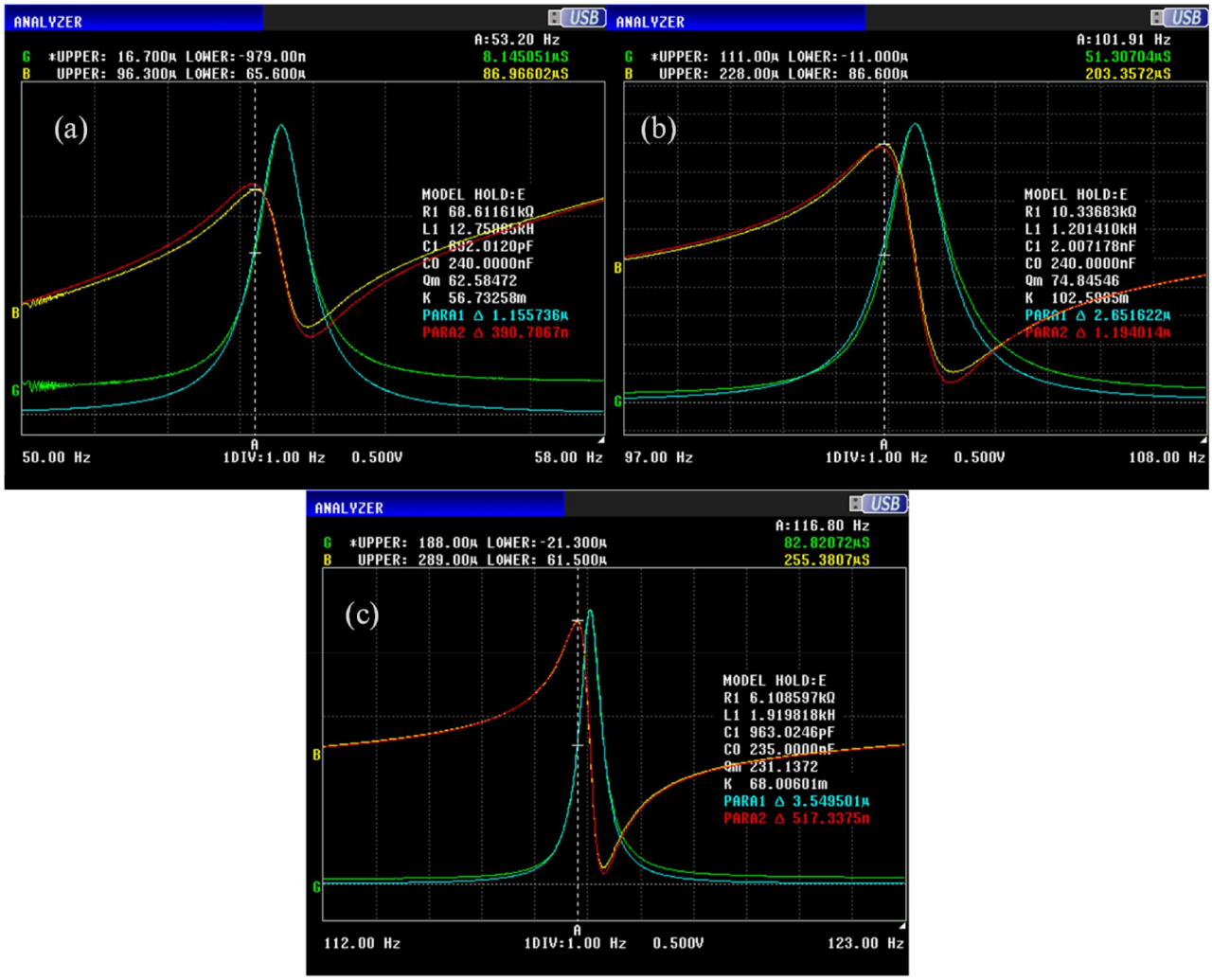

Figure 6. Measured admittance of (a) PZT-1 around the first natural frequency, (b) PZT-1 around the second natural frequency, and (c) PZT-2 around the third natural frequency.

scaling factor for each vibration mode is summarized at Table 2.

Multiplying the scaling factors with the arbitrary eigenvectors yields the mass-normalized mode shapes for every degree of freedom within the structure. These mass-normalized mode shapes were obtained by applying each vibration mode's scaling factor to the measured arbitrary mode shape at 21 different test points using experimental modal analysis (EMA). For validation purposes, a finite element model of the experimental setup is developed using ANSYS software. The FE modal analysis was carried out to obtain the mass normalized mode shapes of the structure. The results of finite element simulation and experimental modal analysis are compared in Figure 7. The experimental result of first, second, and third vibration modes are perfectly matched with the FE results.

The Modal Assurance Criterion (MAC) serves as a valuable tool for assessing the degree of similarity between modal vectors obtained through experimental modal testing and those derived from finite element analysis. As the MAC value approaches 1, it strongly suggests a high level of correlation between the two vectors, while the MAC value near 0, represents a strong indication that the two vectors are very uncorrelated. Figure 8 indicates the MAC metric of EMA and FE. The MAC value of EMA and FE eigenvectors at each vibration mode are close to one i.e. 0.98, 0.99, 0.96 for mode1, mode2, and mode3, respectively. On the other hand, the MAC values of each vibration mode and other two vibration modes are near zero. This proves that the mode shapes are linearly independent where the orthogonality of them are satisfied. It can be concluded that the presented methodology to mass normalize mode shapes of the structure offers a robust and effective approach and provides accurate scaling factors.

The proposed methodology assumes linear system behavior and moderate damping, which ensures accurate extraction of modal parameters. While experimental uncertainties and environmental factors may introduce minor variations, the approach remains applicable as each structure is treated as an independent system. To improve accuracy, careful sensor placement, calibration, and appropriate signal processing techniques are recommended. Automating the measurement and processing steps could enhance efficiency, making the method more practical for applications such as structural health monitoring. Future research could focus on enhancing the methodology for highly damp or nonlinear systems

Table 2. Measured parameters and identified mass normalizing scale factor.

Parameter	Mode 1	Mode 2	Mode 3
Equivalent resistance R_m (Ω)	68,611.6	10,336.8	6108.6
Equivalent inductance L_m (H)	12,759.8	1201.4	1919.8
Resonance frequency ω_m $\left(\frac{rad}{sec}\right)$	337.47	645.47	733.87
Charge FRF $\tilde{H}_{(j\omega_m)}$ $\left(\frac{C}{N}\right)$	1.308e − 6	1.46e − 6	3.69e − 6
Arbitrary mode shape of the reference point $\Phi_m(x_0, y_0)$	3.1682	8.28	33.94
Mass normalized mode shape of the reference point $\varphi_m(x_0, y_0)$	0.268	0.281	0.3776
Scaling factor	0.08464	0.03391	0.011125

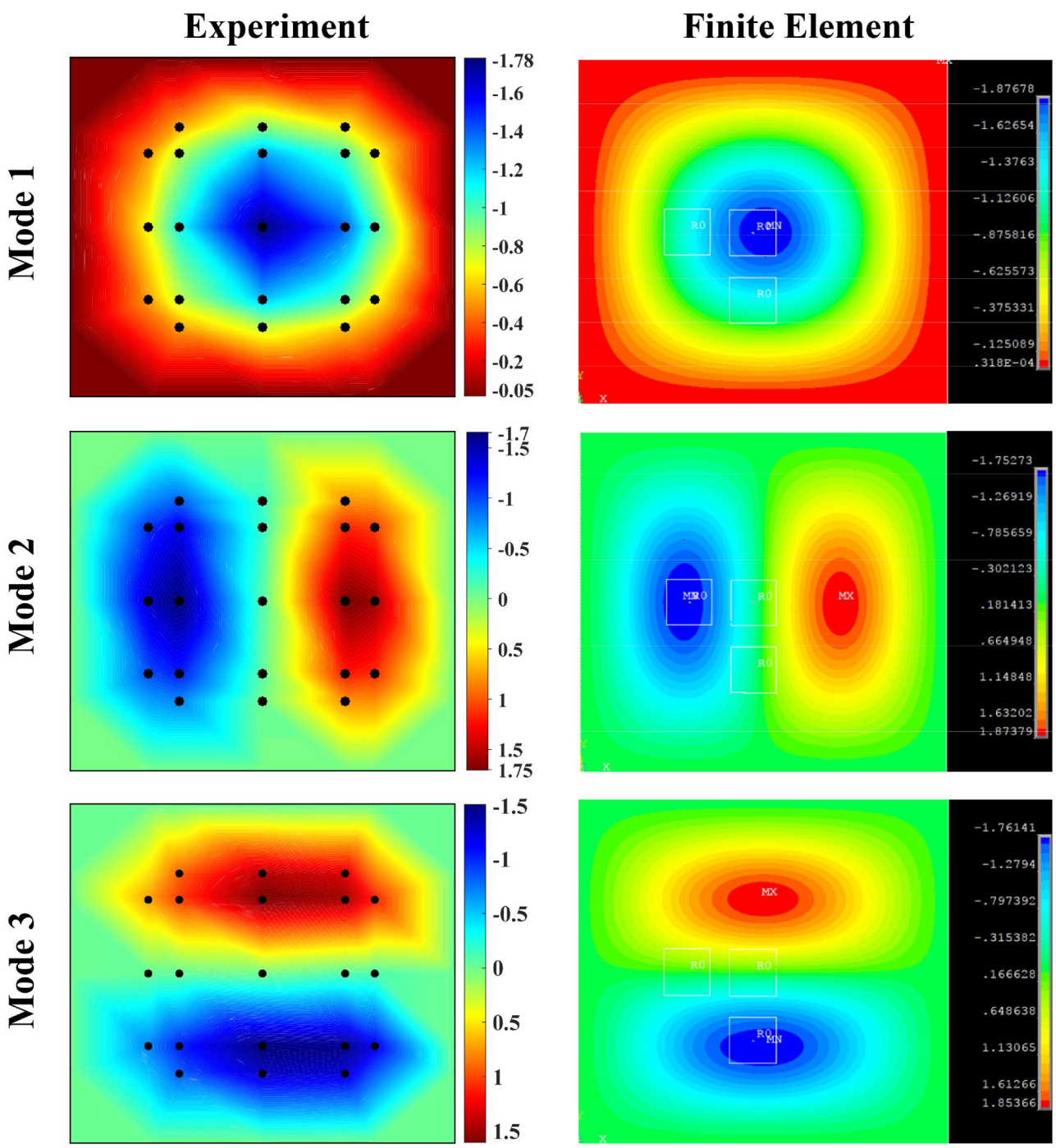

Figure 7. Comparison of mass normalized mode shapes obtained from experimental modal analysis and finite element simulation for three first vibration modes of structure.

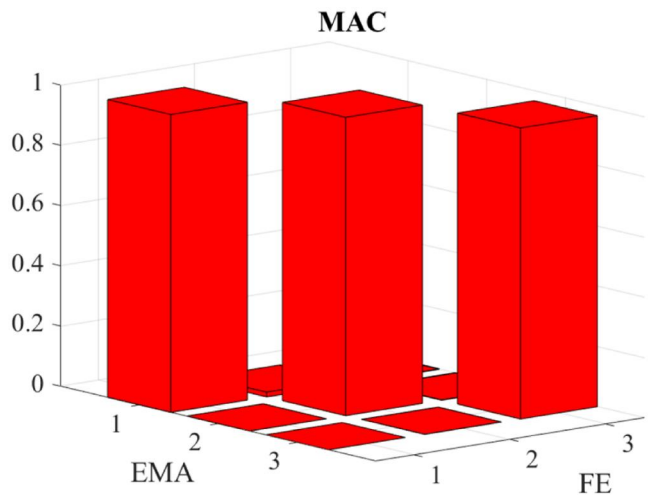

Figure 8. Modal assurance criterion.

which could further extend its applicability. Sensitivity analysis on experimental uncertainties and environmental influences would help refine the approach and improve reliability.

5. Conclusion

Mass normalized mode shapes as an invariant characteristic of structures offer a more precise depiction of a structure's dynamic behavior. Identification of mass normalized mode shapes of a structure is challenging, and several methodologies have been presented to overcome this problem. However, the proposed methodologies have some drawbacks. Mass-change methodology can affect the dynamic behavior of the structure which leads to inaccurate prediction of the structure's modal parameters. Moreover, the conventional experimental modal analysis method requires precise calculation of the modal parameters and dealing with complex equations. Therefore, this paper presents an alternative approach which does not affect the dynamic behavior of the structure during the experimental measurements. Additionally, the methodology avoids excessive calculations on the measurement data and provides a robust and straightforward approach to accurately predict mass-normalizing scale factors for each vibration mode of thin-walled structures, such as beams and plates. The presented methodology uses electromechanical impedance measurement and the charge FRF of a piezoelectric transducer attached to the structure to acquire the mass normalized mode shape of the reference point (force location). By mechanically exciting the structure and measuring the mechanical response of the structure at the reference point, the arbitrarily scaled mode shape can be obtained. The scaling factor for each vibration mode is then determined by comparing the arbitrary mode shape with the mass-normalized one at the reference point, allowing for the computation of the mass-normalized mode shapes of the entire structure.

The presented methodology was examined by a fully clamped aluminum plate. The plate was excited by a swept sine input force to obtain the acceleration FRF of 21 test points. The imaginary part of the acceleration FRFs provided the arbitrarily scaled mode shapes of the structure. Similarly, the acceleration FRFs of the reference points and the charge FRFs of the piezoelectric patches are measured. An impedance analyzer was used to acquire the piezoelectric admittance and equivalent electrical properties. Subsequently, the component of the mass normalized mode shape at the reference point and the scaling factor for each vibration mode is calculated. Having the scaling factors, the mass normalized mode shapes of the structure are calculated. The results are compared with the mass normalized mode shapes obtained from a finite element analysis where a good agreement between the results is shown. In order to assess the degree of similarity between the modal vectors obtained through experimental modal testing and finite element analysis, modal assurance criterion (MAC) was calculated. Based on the MAC values, it was proved that the proposed methodology predicts the mass normalized mode shapes accurately which provides a robust and accurate approach for mass normalization of the mode shapes in transversely vibrating structures.

Disclosure statement

No potential conflict of interest was reported by the author(s).

References

[1] Y. Wang, M. Liang, and J. Xiang, Damage detection method for wind turbine blades based on dynamics analysis and mode shape difference curvature information, Mech. Syst. Sig. Process., vol. 48, no. 1-2, pp. 351–367, 2014. DOI: 10.1016/j.ymssp.2014.03.006.

[2] K. Schuster, U. Kowalsky, and D. Dinkler, System identification and structural health monitoring using piezoceramic actuators, Mech. Adv. Mater. Struct., vol. 18, no. 7, pp. 540–547, 2011. DOI: 10.1080/15376494.2011.605014.

[3] G.F. Gomes, Y.A.D. Mendéz, P. da Silva Lopes Alexandrino, S.S. da Cunha, and A.C. Ancelotti, The use of intelligent computational tools for damage detection and identification with an emphasis on composites – A review, Compos. Struct., vol. 196, pp. 44–54, 2018. DOI: 10.1016/j.compstruct.2018.05.002.

[4] Y. Du, S. Zhou, X. Jing, Y. Peng, H. Wu, and N. Kwok, Damage detection techniques for wind turbine blades: a review, Mech. Syst. Sig. Process., vol. 141, pp. 106445, 2020. DOI: 10.1016/j.ymssp.2019.106445.

[5] G. Zhang, L. Tang, Z. Liu, L. Zhou, Y. Liu, and Z. Jiang, Machine-learning-based damage identification methods with features derived from moving principal component analysis, Mech. Adv. Mater. Struct., vol. 27, no. 21, pp. 1789–1802, 2020. DOI: 10.1080/15376494.2019.1710308.

[6] G.F. Gomes, Deep learning enhanced metamodel design based on reduced mode shapes for delamination identification in composite structures, Mech. Adv. Mater. Struct., vol. 31, no. 29, pp. 11221–11238, 2024. DOI: 10.1080/15376494.2024.2302921.

[7] D.J. Ewins, Modal Testing: Theory, Practice and Application, John Wiley & Sons, Baldock, Hertfordshire, England, 2009.

[8] M. Sheibani and A.K. Ghorbani-Tanha, Obtaining mass normalized mode shapes of motorway bridges based on the effect of traffic movement, Structures, vol. 33, pp. 2253–2263, 2021. DOI: 10.1016/j.istruc.2021.05.056.

[9] Y. He, J.P. Yang, and Z. Yan, Estimating modal scale factors based on vehicle-induced variation of bridge frequencies, Eng.

Struct., vol. 277, pp. 115424, 2023. DOI: 10.1016/j.engstruct.2022.115424.

[10] P. Avitabile, Modal Testing: A Practitioner's Guide, John Wiley & Sons, 2017. DOI:10.1002/9781119222989

[11] E. Carrera, R. Augello, and K. Abu Salem, Evaluation of the effects of different materials on the dynamic properties of thin-walled metamaterial structures, Mech. Adv. Mater. Struct., vol. 31, pp. 1–16, 2024. DOI: 10.1080/15376494.2024.2434194.

[12] R. Volkmar, K. Soal, Y. Govers, and M. Böswald, Experimental and operational modal analysis: Automated system identification for safety-critical applications, Mech. Syst. Sig. Process., vol. 183, pp. 109658, 2023. DOI: 10.1016/j.ymssp.2022.109658.

[13] A. Messina, Local diagnoses in modal analysis through additional poles, Mech. Adv. Mater. Struct., vol. 28, no. 9, pp. 928–937, 2021. DOI: 10.1080/15376494.2019.1614704.

[14] F. Boumediene, F. Bekhoucha, and E.-M. Daya, Modal analysis of rotating viscoelastic sandwich beams, Mech. Adv. Mater. Struct., vol. 28, no. 4, pp. 405–417, 2021. DOI: 10.1080/15376494.2019.1567887.

[15] E. Gülbahçe and M. Çelik, Experimental modal analysis for the plate structures with roving inertial shaker method approach, J. Low Freq. Noise. Vibr. Act. Control, vol. 41, no. 1, pp. 27–40, 2022. DOI: 10.1177/14613484211039323.

[16] C.M. Pappalardo, Şİ. Lök, L. Malgaca, and D. Guida, Experimental modal analysis of a single-link flexible robotic manipulator with curved geometry using applied system identification methods, Mech. Syst. Sig. Process., vol. 200, pp. 110629, 2023. DOI: 10.1016/j.ymssp.2023.110629.

[17] L. Liu, F. Ripamonti, R. Corradi, and Z. Rao, On the experimental vibroacoustic modal analysis of a plate-cavity system, Mech. Syst. Sig. Process., vol. 180, pp. 109459, 2022. DOI: 10.1016/j.ymssp.2022.109459.

[18] M.M. Rosso, A. Aloisio, J. Parol, G.C. Marano, and G. Quaranta, Intelligent automatic operational modal analysis, Mech. Syst. Sig. Process., vol. 201, pp. 110669, 2023. DOI: 10.1016/j.ymssp.2023.110669.

[19] F. Magalhães, Á. Cunha, E. Caetano, and R. Brincker, Damping estimation using free decays and ambient vibration tests, Mech. Syst. Sig. Process., vol. 24, no. 5, pp. 1274–1290, 2010. DOI: 10.1016/j.ymssp.2009.02.011.

[20] P. Avitabile, Modal space: Someone told me that operating modal analysis produces better results and that damping is much more realistic, Exp. Tech., vol. 30, no. 6, pp. 25–26, 2006. DOI: 10.1111/j.1747-1567.2006.00102.x.

[21] E. Orlowitz and A. Brandt, Comparison of experimental and operational modal analysis on a laboratory test plate, Measurement, vol. 102, pp. 121–130, 2017. DOI: 10.1016/j.measurement.2017.02.001.

[22] E. Parloo, P. Verboven, P. Guillaume, and M. Van Overmeire, Sensitivity-based operational mode shape normalisation, Mech. Syst. Sig. Process., vol. 16, no. 5, pp. 757–767, 2002. DOI: 10.1006/mssp.2002.1498.

[23] E. Parloo, B. Cauberghe, F. Benedettini, R. Alaggio, and P. Guillaume, Sensitivity-based operational mode shape normalisation: Application to a bridge, Mech. Syst. Sig. Process., vol. 19, no. 1, pp. 43–55, 2005. DOI: 10.1016/j.ymssp.2004.03.009.

[24] T. Kranjc, J. Slavič, and M. Boltežar, The mass normalization of the displacement and strain mode shapes in a strain experimental modal analysis using the mass-change strategy, J. Sound Vib., vol. 332, no. 26, pp. 6968–6981, 2013. DOI: 10.1016/j.jsv.2013.08.015.

[25] M.M. Khatibi, M.R. Ashory, A. Malekjafarian, and R. Brincker, Mass–stiffness change method for scaling of operational mode shapes, Mech. Syst. Sig. Process., vol. 26, pp. 34–59, 2012. DOI: 10.1016/j.ymssp.2011.07.012.

[26] M.L. Aenlle and R. Brincker, Modal scaling in operational modal analysis using a finite element model, Int. J. Mech. Sci., vol. 76, pp. 86–101, 2013. DOI: 10.1016/j.ijmecsci.2013.09.003.

[27] W.-Y. He, W.-X. Ren, and X.-H. Zuo, Mass-normalized mode shape identification method for bridge structures using parking vehicle-induced frequency change, Struct Control Health Monit., vol. 25, no. 6, pp. e2174, 2018. DOI: 10.1002/stc.2174.

[28] R. Nayek, S. Mukhopadhyay, and S. Narasimhan, Mass normalized mode shape identification of bridge structures using a single actuator-sensor pair, Struct Control Health Monit, vol. 25, no. 11, pp. e2244, 2018. DOI: 10.1002/stc.2244.

[29] X. Guo, Z. Su, and L. Wang, Active boundary control of spinning beams with elastic constraints using piezoelectric stack actuator, Mech. Adv. Mater. Struct., vol. 31, pp. 1–10, 2024. DOI: 10.1080/15376494.2024.2427921.

[30] J. Najd, E. Zappino, E. Carrera, W. Harizi, and Z. Aboura, Optimal position and dimensions of embedded normal piezoelectric transducers, higher order plate models and experimental approach, Mech. Adv. Mater. Struct., vol. 31, no. 27, pp. 9887–9898, 2024. DOI: 10.1080/15376494.2024.2342028.

[31] S.M. Hoseyni, M. Simsek, A. Aghakhani, E. Lefeuvre, and I. Basdogan, Multimodal piezoelectric energy harvesting on a thin plate integrated with SSHI circuit: an analytical and experimental study, Smart Mater. Struct., vol. 32, no. 9, pp. 095024, 2023. DOI: 10.1088/1361-665X/ace9a0.

[32] J. Qiu, X. Yuan, Q. Lv, H. Xu, D. Li, and Q. Wen, Geometrically nonlinear wind-induced vibration piezoelectric energy harvester based on vortex-induced vibration, Mech. Adv. Mater. Struct., vol. 31, pp. 1–9, 2024. DOI: 10.1080/15376494.2024.2417355.

[33] L. Zhao, Y. Gong, F. Shen, H. Wu, Y. Peng, S. Xie, and Z. Li, Effect of stability state transition of variable potential well in tri-hybridized energy harvesters, Mech. Syst. Sig. Process., vol. 223, pp. 111855, 2025. DOI: 10.1016/j.ymssp.2024.111855.

[34] E. Tarhan, S.M. Hoseyni, A. Aghakhani, and I. Basdogan, Investigation of networked SSHI configurations for plate-based piezoelectric energy harvesters, J. Intell. Mater. Syst. Struct., 1045389X241306534, vol. 36, 2025. DOI: 10.1177/1045389X241306534.

[35] M. Ali, S.M. Hoseyni, R. Das, M. Awais, I. Basdogan, and L. Beker, A flexible and biodegradable piezoelectric-based wearable sensor for non-invasive monitoring of dynamic human motions and physiological signals, Adv. Mater. Technol., vol. 8, no. 15, pp. 2300347, 2023. DOI: 10.1002/admt.202300347.

[36] G. Piana, E. Lofrano, A. Carpinteri, A. Paolone, and G. Ruta, Experimental modal analysis of straight and curved slender beams by piezoelectric transducers, Meccanica, vol. 51, no. 11, pp. 2797–2811, 2016. DOI: 10.1007/s11012-016-0487-y.

[37] U. Aridogan, I. Basdogan, and A. Erturk, Analytical modeling and experimental validation of a structurally integrated piezoelectric energy harvester on a thin plate, Smart Mater. Struct., vol. 23, no. 4, pp. 045039, 2014. DOI: 10.1088/0964-1726/23/4/045039.

[38] A. Aghakhani and I. Basdogan, Equivalent impedance electroelastic modeling of multiple piezo-patch energy harvesters on a thin plate with AC–DC conversion, IEEE/ASME Trans. Mechatron., vol. 22, no. 4, pp. 1575–1584, 2017. DOI: 10.1109/TMECH.2017.2712713.

[39] S.M. Hoseyni, A. Aghakhani, and I. Basdogan, Experimental admittance-based system identification for equivalent circuit modeling of piezoelectric energy harvesters on a plate, Mech. Syst. Sig. Process., vol. 208, pp. 111016, 2024. DOI: 10.1016/j.ymssp.2023.111016.